www.czasopisma.pan.pl PAN POLSKA AKADEMIA NAUK www.journals.pan.pl

Arch. Metall. Mater. **64** (2019), 4, 1569-1575

DOI: 10.24425/amm.2019.130128

YU LIU*,***#, YUANCHUN HUANG*,**,***#, ZHENGBING XIAO*,***

AMOUNT AND DISTRIBUTION OF MICRO-DEFECTS IN SOLIDIFIED 2219 Al ALLOY INGOTS: A METALLOGRAPHIC INVESTIGATION

Micro-defects detection in solidified castings of aluminum alloy has always been a hot topic, and the method employed is mainly depends upon the size and shape of the specimens. In present paper, the amount and distribution characters of micro-defects in a series of 2219 aluminum alloy ingot, with diameters of φ1380 mm, φ1250 mm, φ1000 mm, φ850 mm and φ630 mm, prepared by direct chill casting were investigated by means of metallographic, respectively. Samples were cut along the radius direction from slices in the steady casting stage. The result reveals that typical micro-defects are consist of inclusions, porosity and shrinkage under optical microscope, and the total amount of micro-defect per unit area in an ingot slightly decreased with the increase of its diameter. Meanwhile, defects were classified into 2 types according to its size, the results suggesting that defects greater than 40 μm account for the largest proportion among the counted two kinds of defects. Moreover, the distribution of defects greater than 40 μm along the radial direction was detected, its amount increases as its distance from the side, indicating that the micro-defects greater than 40 μm distributed the most in the center zone of ingots and the larger the ingot diameter, the more obvious the tendency was.

Keywords: metallographic, micro-defect, 2219 Al alloy ingot, amount, distribution

1. Introduction

2219 aluminum alloy has been widely used in a range of aerospase applications such as high temperature structural applications including space booster and fuel tanks for its excellent weldability, workability and mechanical properties at low and high temperature, high specific strength and fracture toughness and good stress corrosion resistance [1,2]. And one of its typical application is to manufacture ring component and skin that serviced in rockets [3]. As commonly recognized that representative processing procedures of a wrought aluminum alloy component including casting, homogenization, plastic deformation (extrusion, rolling, forging, etc.), solution and aging treatment. Obviously, casting is the first step of the whole process for the manufacturing of a component, more and more attention has been aroused on the quality control of castings in the past decades [4,5]. The micro-defects in a solidified aluminum alloy ingot is considered to be a important subject to evaluate the quality of an ingot, since its size, amount and distribution plays a key role in determining the workability and the microstructure evolution in the processing steps, especially for the plastic deformation behaviors, and the properties of final products [6,7]. As reported, the formation of micro-defect is mainly attributes to the evolution of residual gases and inclusions, meanwhile, the phase transformation during the solidification process may lead to another defect, known as shrinkage [6,8-10]. Thus, many efforts have been devoted to lower the gas and inclusions content before casting as much as possible, mainly focused on furnace fluxing, on-line degassing and filtration. Also, many products were developed, such as Rotary flux injection (RFI) [11], Rotary Gas injection (RGI) [12], Spinning Nozzle Inert Floatation (SNIF) [13], and Deep-Bed Filtration [14], accordingly.

On the other hand, assessing the quality of melt and castings has always been a hot topic, and have attracted many focuses. Up to now, many researches have been performed on the detection of inclusions and hydrogen in molten melt, and several devices have been developed, such as HYSCAN [15], LIMCA [16], PodFA [17], and Prefil Footprinter [18]. But these methods were employed to characterize the quality of the melt, e.g. type, size, amount of inclusions and concentration of hydrogen, and some of them are either expensive or time consuming. Meanwhile, several methods have also been proposed to evaluate the quality of solidified castings, among which one of the main aspects was the assessment of micro-defects.

X-ray radiography is a kind of non-destructive technique, based on the different refractive properties of components in a given material system to X-rays, to assess casting quality, it can be used to distinguish inclusions, pores, internal cracks and shrinkage

* CENTRAL SOUTH UNIVERSITY, RESEARCH INSTITUTE OF LIGHT ALLOY, CHANGSHA, 410083, CHINA
** CENTRAL SOUTH UNIVERSITY, COLLEGE OF MECHANICAL AND ELECTRICAL ENGINEERING, CHANGSHA 410083, CHINA
*** CENTRAL SOUTH UNIVERSITY, NONFERROUS METAL ORIENTED ADVANCED STRUCTURAL MATERIALS AND MANUFACTURING COOPERATIVE INNOVATION CENTER, CHANGSHA, 410083, CHINA
# Corresponding author: csuliuyu@csu.edu.cn, science@csu.edu.cn

[19,20]. X-ray radiography allows to detect the morphology and relative position of micro-defects in castings in the case of the X-rays could transmit through the whole sample, thus, thick samples can be fully interrogated only with high-energy X-ray sources. So it is commonly employed to test small or thin samples. X-ray tomography is another use of X-rays, with which a 3D image of the testing samples can be obtained, and there's no need to cut and polish the samples [21]. Thus, the morphology, size distribution, position, and volume fraction of inclusions within the sample can be accurately obtained from the 3D image. Similarly, X-ray tomography is applicable only to small size samples, owing to the transmitting properties of X-rays, and the cost is high. Up to now, it is more of a laboratory-based detection method [22].

Ultrasound is also being used to exam defects in solid castings, it allows to detect defects of voids, pores, cracks, and inclusions [23,24]. With the sound pulse, generated by a transducer toward the sample surface, propagates in the sample, a reflected signal will be collected by the transducer again when the pulse encounters a defects. Depending on the portion of the reflected pulse, one can obtain the size and shape features of the detected defects over the entire sample area. Although this technique has no need to prepare samples, but the resolution of the detected defects was limited by the penetration depth of the pulse, so it only yield to small and thin samples [22].

Metallography is a traditional method to examine defects in solidified castings, the sample was cut, polished, and examined under an optical microscope. With a image analysis system, one can quantitative analyses the size, distribution and area fraction of defects, meanwhile, samples can also be analyzed chemically via energy-dispersive spectroscopy on the scanning electron microscope. Thus, the defects present in a casting could be fully understood by combination chemistry, concentration, size and distribution. However, this method also has its limitations, the preparation for samples seems time consuming and the examination results can not fully reflect the whole casting as only limited samples and a small area were analyzed. Nonetheless, it is a good choice for large-scale cylindrical ingot with symmetrical structure. Therefore, in present paper, the micro-defects analysis to a series ingot of 2219 aluminum alloy prepared by direct chill casting, which were used for the manufacturing of rings, were performed with metallographic method. Both amount and distribution characters along the radius direction were examined for the section in the steady casting stage.

2. Experimental procedures

2.1. Materials and samples preparation

In present paper, 2219 aluminum alloy containing 6.3 wt. pct. Cu and 0.3 wt. pct. Mn were selected for micro-defects analyze. The molten melt was purified by fluxing, degassing and filtering before casting. Thereby, a series of ingots, with diameters of φ1380 mm, φ1250 mm, φ1000 mm, φ850 mm and φ630 mm, were prepared by direct chill casting, respectively. In order to avoid the effects of fluctuation, in the beginning stage of casting, on the micro-defects of as-cast ingot, we investigate the solidified ingot in the steady casting state. Accordingly, cross-sectional slices of the ingot with a total thickness of 30 mm were cut in transverse direction at 770 mm from the top of ingot, as Fig. 1(a) shows.

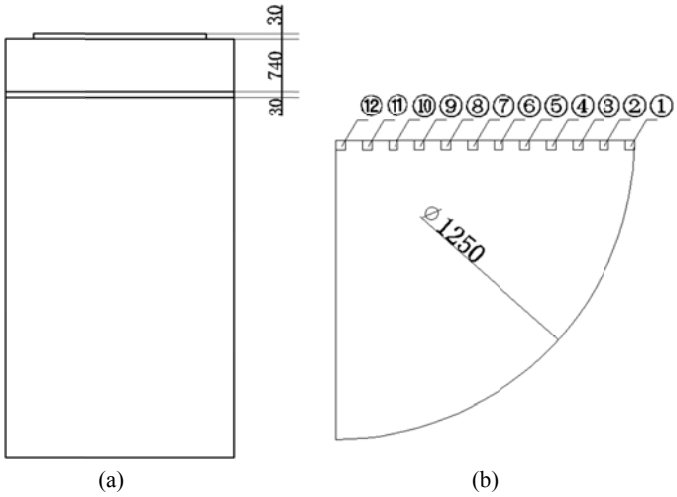

Fig. 1. Schematic of sampling positions: (a) analyzed slice positions along the length of the ingot; (b) sample positions along the radius direction of the 1250-mm diameter ingot

To investigate the distribution of micro-defects, specimens with the size of 10×10-mm^2 were cut along the radius direction for about every fifty millimeters on the obtained slices. As an example, Fig. 1 (b) shows the sampling positions along the radius direction for 1250-mm diameter ingot. Thus, 14, 12, 10, 9 and 6 samples were cut from 1380-mm, 1250-mm, 1000-mm, 850-mm and 630-mm diameter ingot slices along the radius direction, respectively.

2.2. Analysis method

The microscopic observation was carried out on the obtained samples, that cut from the slices after polished, using an optical microscope of Olympus DSX500 and a scanning electron microscope equipped with an energy-dispersive X-ray spectrometer. After test, 16 single graphes, consist of 4 sets contiguous photos along the vertical direction and each set contains 4 contiguous photos along the horizontal direction, were captured for each sample under the magnification of 200X to cover the center zone of specimen for about 25 mm^2. Then the collected single graphs were mosaicked into one whole image with an image analysis system. Thirdly, threshold segmentation based on pixels grey-scale was carried out with the assistance of a program, and the pictures were separate into two parts, i. e. defect area and nondefect area. Thus, we counted the defects regardless of its type, then quantitative analysis and the distribution characteristics of micro-defects along the radius direction in solidified aluminum ingots could be gained.

3. Results and discussion

3.1. Morphology of typical defects

Fig. 2 shows the morphology of typical defects in a solidified ingot under optical microscope, as can be obviously seen from the figure that the micro-defects presented differently from matrix, based on which the identification and extraction of micro-defects were performed later. Further research of morphology of typical defects in ingots were also performed with SEM, thus, the morphology of typical micro-defects under scanning electron microscope are clearly presented in Fig. 3. As can be seen from Fig. 3, apart from inclusions, pores are main defect that occurred in solidified castings, and pores predominantly caused by gas with a smoother boundary (Fig. 3(c)), while pores predominantly caused by shrinkage with a less smooth boundary (Fig. 3(b)). Thereby, typical morphology of various types of micro-defects, which consist of inclusions and porosity were investigated with OM and SEM/EDS for the studied 2219 aluminum alloy.

Accordingly, shrinkage is observed under scanning electron microscope, around which the elemental distribution was analyzed with EDS, and the results are present in Fig. 4. As can be seen from Fig. 4, element of Oxygen (O), Copper (Cu) and Aluminum (Al) are distributed in the analyzed area, and the elemental compositions of the inclusions are O and Al. It can be gained that the inclusion cluster mainly consist of oxides.

As presented above micro-defects are mainly consist of inclusions and porosity (usually classified as gaseous and shrinkage). The micro-defects, in the form of inclusions and gaseous, are mainly owing to the evolution of remained inclusions and

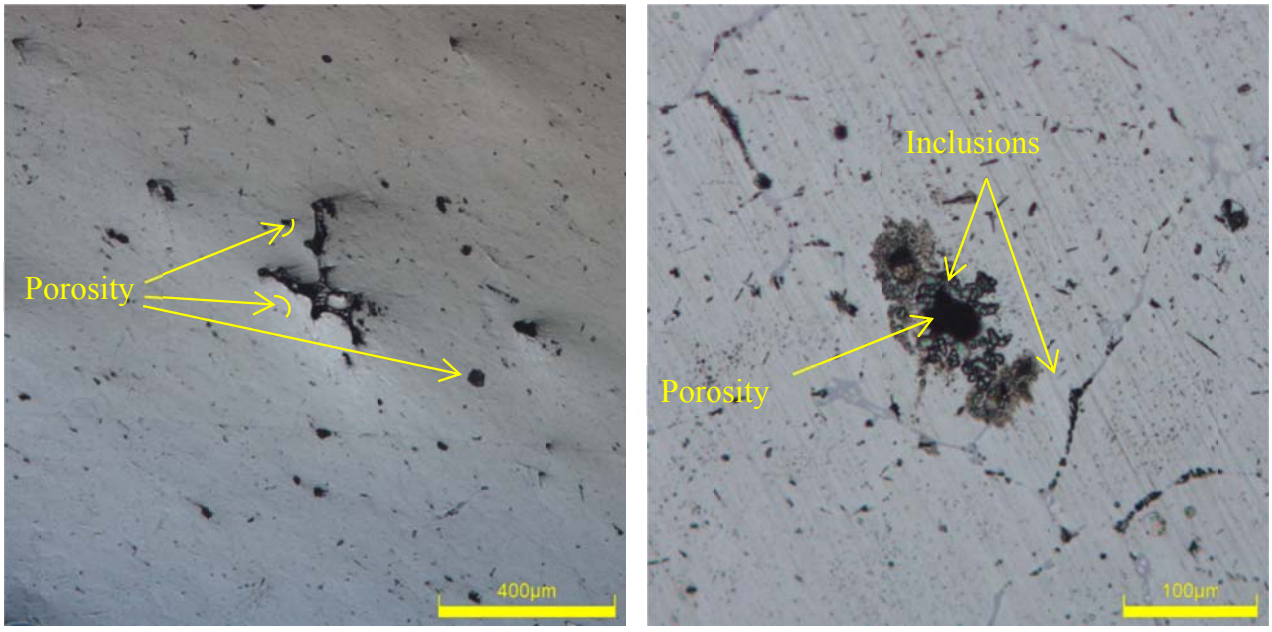

Fig. 2. Morphology of typical micro-defects under optical microscope

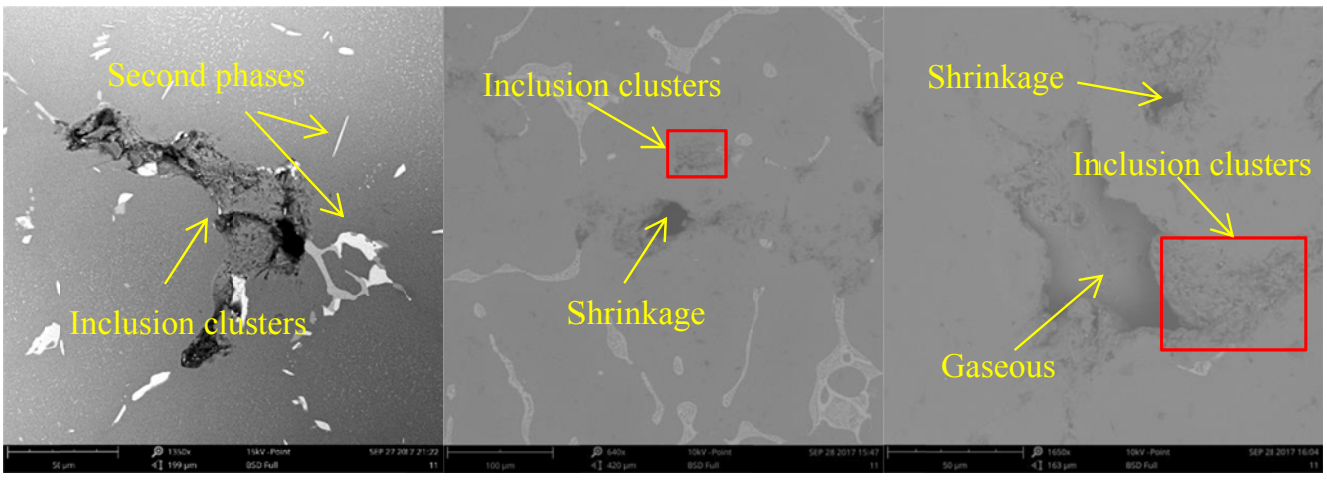

Fig. 3. Morphology of typical micro-defects under scanning electron microscope

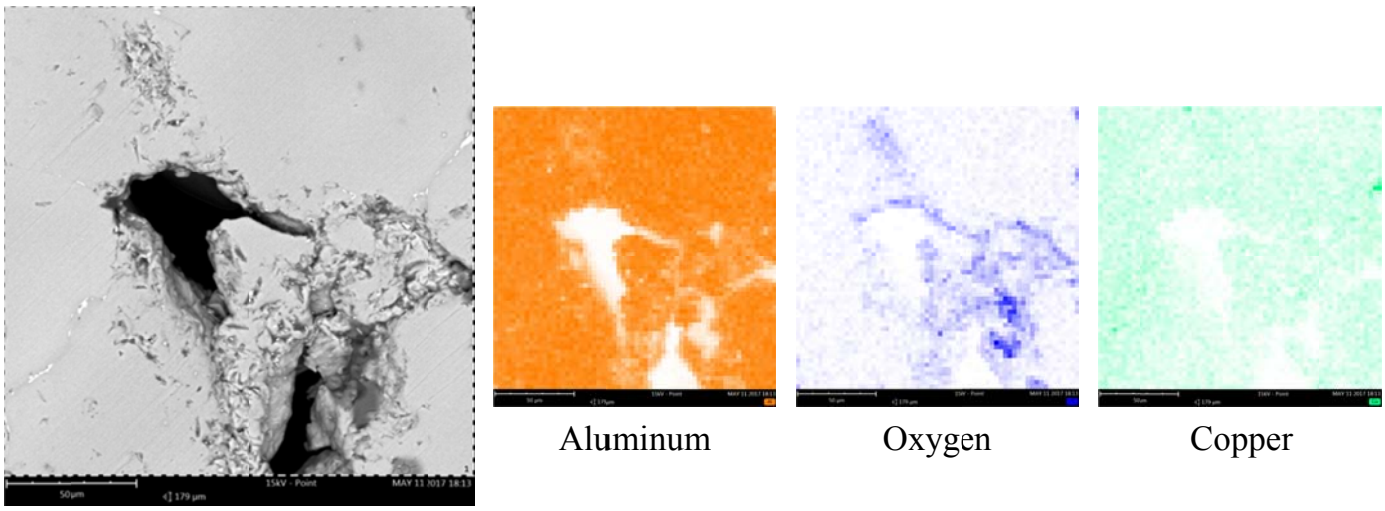

Fig. 4. Element Map of region around a porosity defect using EDS on SEM

hydrogen in the melt before casting. As recognized, large size inclusions were removed after filtration treatment, however, the inclusions in small sizes collided and aggregated under the motions of melt in mould, and tend to gather into big one during the casting process, then the coarsened inclusions evolved into the solidified ingot is visible under optical microscope [25]. Thus, the increase of the inclusions content of the melt promotes the formation of inclusions in ingot. Meanwhile, the gases dissolved in the molten melt precipitates gradually as the temperature decreases, the released gases diffused and transferred to the residual liquid between the dendrite arms, causing the gas in the local area to be supersaturated to form bubbles [26]. However, under the circumstances of rapid solidification, the bubbles can not escape in time for the resistance of primary dendrites and dendrite arms, then the amount of gas bubbles escaping from the melt is limited, and the remaining bubbles tend to form gaseous. The formation of gaseous occurs in the liquid state or during the early stage of solidification, and the shape of porosity is spherical or ellipsoid [27]. Thus, the increase of the gas content of the melt promotes the formation of the porosity.

In contrast to gaseous, the shrinkage tend to appear at the end of solidification range, and the shape is related to the remaining space between the dendrites [28], and is very tortuous for the most time. Generally, the shrinkage of the solidified areas, as the temperature decreased, can be compensated by feeding melt in the mushy zone, but it is difficult for a wide range mushy zone as the restraint of the fluid flow in the mushy zone, the melt can not be sufficient down to the root of the dendrite, which leads to an insufficient feeding, and, to the formation of shrinkages.

On the other hand, the remaining inclusions tend to increase viscosity of the melt and further hinders the flowability of the melt, which decrease the escaping speed of rising bubbles and feeding capacity of the melt, and accordingly promote gaseous and shrinkage. Thus, with the regard of defects caused by inclusions and gaseous, to remove inclusions and hydrogen from molten melt before casting is the only way to avoid these defects. Addtionally, the optimization of casting parameters is an effective way to control micro-defects of shrinkage, and a low depth molten hole is preferable to decrease shrinkage.

3.2. Area fraction of micro-defects and its distribution

As mentioned above, micro-defects were observed and captured with an optical microscope, and defects were classified into two types according to their diameter. Herein, defects diameter of 10~40 μm and greater than 40 μm were counted and analyzed in present study. It is necessary to note that we omitted defects that smaller than 10 um- diameter when analyze the defects, as scratches, stains, grain boundaries or phase components could be incorrectly classified as casting defects for its small size. Thereby, a typical microphotograph consist of 16 single images of 630-mm diameter ingot, which were took from the same specimen as introduced above, is present in Fig. 5(a). As can be seem from the figure that typical defects and its distribution are clearly presented, additionally, the image are similar to the results observed in other studied ingots. Meanwhile, the micro-defects in the matrix were highlighted by adjusting threshold value of the picture, as Fig. 5(b) shows. Thus, the micro-defects, black areas in Fig. 5(a) (i. e. the green areas in Fig. 5(b)), were counted and sorted into two kinds according to the defects diameter. The area fraction of micro-defects was defined and calculated with the following formula,

$$c = \frac{A_{md}}{A_{total}} \times 100\%$$

Where c is the area fraction of micro-defect, A_{total} is the total analyzed area, A_{md} is the area of micro-defect in the analyzed area.

Fig. 6 show the area fraction of micro-defects of 10~40-μm, >40-μm diameter in different samples that distributed along radius direction of 1380-mm, 1250-mm, 1000-mm, 850-mm and

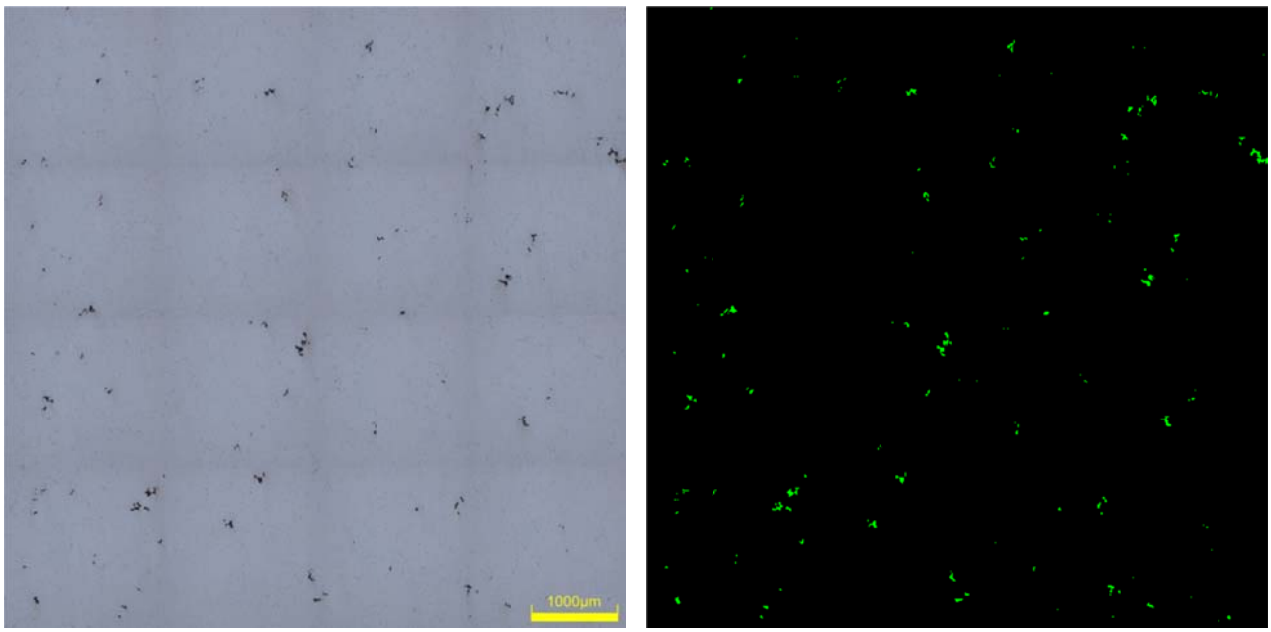

(a) **(b)**

Fig. 5. Stitching diagram of acquisition and extraction for micro-defects of ingot, (a) micro-defect acquisition, (b) micro-defect extraction

630-mm diameter ingot, respectively, along with the total area fraction of the above two kinds of defects. Accordingly, several remarks could be deduced from the presented figures.

Firstly, the total area fraction of micro-defect in an ingot slightly decreased with the increase of its diameter, it means that the defects content in 1380-mm-diameter ingot is less than that of other ingots, and the most in 630-mm-diameter ingot. Secondly, one also can observe that the defects of diameter greater than 40μm account for the largest proportion among the counted two kinds of defects for the studied 5 ingots. However, for the area fraction of defects of 10~40-μm diameter, there isn't much difference along the radial direction for all the studied five ingots. But for the defects of sizes greater than 40 μm, significant difference along the radial direction was detected, its area fraction increases as its distance from the ingot side, that is to say micro-defects greater than 40 μm distributed the most in the center zone of ingots. Meanwhile, this phenomenon is more obvious in large ingot. Another feature could be deduced from the figure is a strong non-monotonic characteristic was presented on defects contents vs. distance from ingot centre along the whole radius, especially for 1380-mm, 1250-mm, 1000-mm and 850-mm diameter ingot.

As reported, the formation of micro-defects of inclusions and porosity are mainly owing to the evolution of remaining inclusions and hydrogen in the mould after purification treatment in the casting period. In a large size ingot, owing to the limited casting speed and large metallic solidifying interface, as well as the deep melt pool in the mould, the released hydrogen atoms and fine inclusions tend to accumulate in the center zone as the solidification interface moves. Thus, micro-defects comparatively tend to occur in the center zone instead of side section for large size ingots. While for the casting of small size ingot, owing to the large cooling strength, fast casting speed and a small radial temperature gradient, the polymerization of released gas and inclusions can only occur in a small range, then the micro-defects in the radial direction and cross section of the solidified ingot distributed uniformly, as the micro-defects distribution characteristics presented in 630-mm diameter ingot. Besides, the amount of released gases was decreased with the increasing of casting speed, thus, the total area fraction of micro-defects in 630-mm diameter ingot is higher than that of other ingots.

With the methods proposed in this work, one can clearly obtain the information of distribution and amount of micro-defects in a solidified ingot, it will help to evaluate the quality of the ingot and to guide the following processings. However, the micro-defects of castings also include composition segregation, course grains, etc., but those are hard to distinguish from the matrix under optical microscope, so the present work only focused on the micro-defects of inclusions, porosities and shrinkages. Further investigation could focus on the detection of micro-defects qualitatively.

4. Conclusions

In present paper, the amount and distribution characters of micro-defects along the radius direction of 2219 aluminum alloy with diameters of φ1380 mm, φ1250 mm, φ1000 mm, φ850 mm and φ630 mm, which were prepared by direct chill casting, were investigated by means of metallographic. Based on the analysis results for samples in the steady casting stage, several remarks were deduced.

1) Typical micro-defects are consist of inclusions, porosity and shrinkage under optical microscope. And the total area fraction of defects of micro-defect in an ingot slightly decreased with the increase of its diameter.

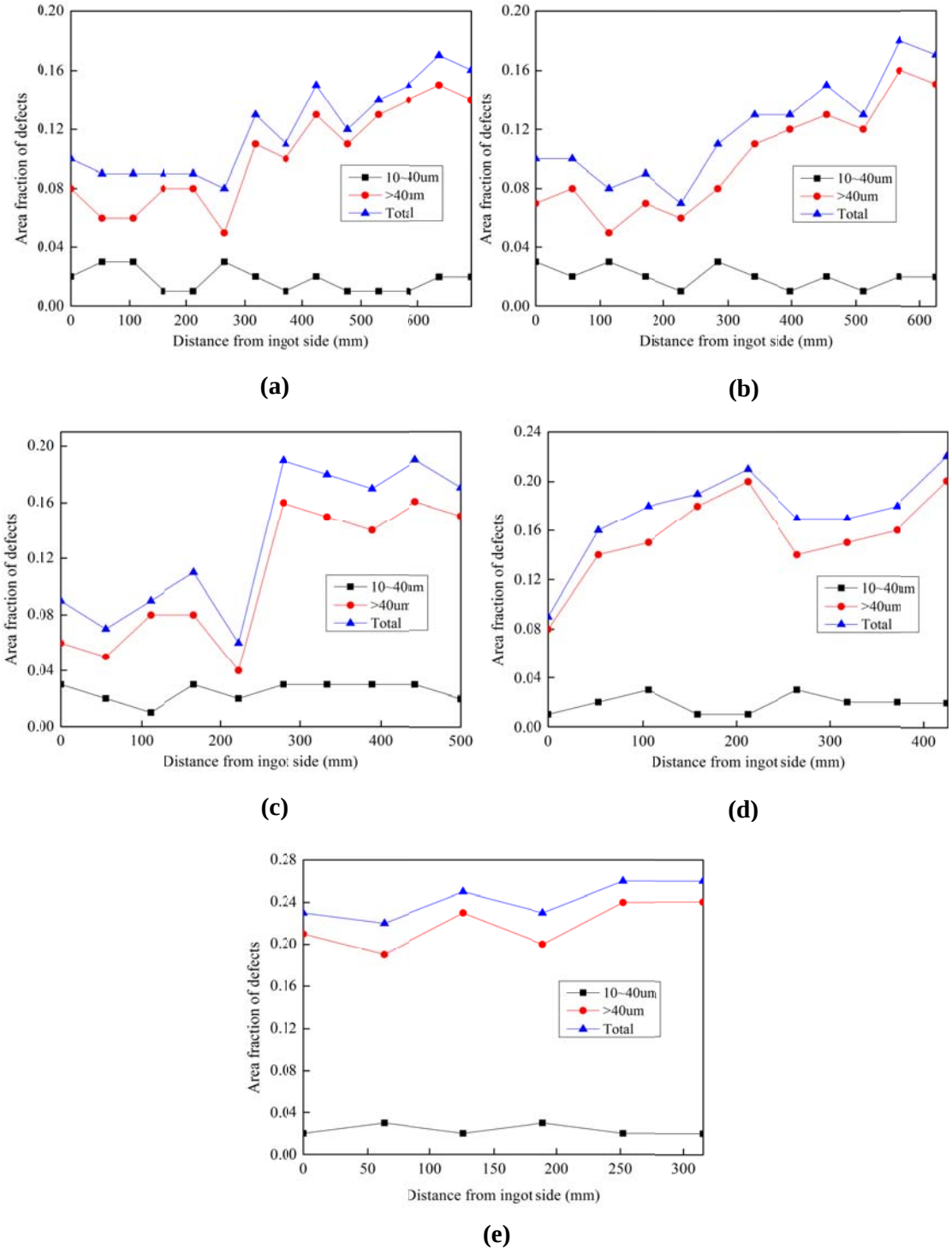

Fig. 6. Area fraction of micro-defects along radius direction of (a) 1380-mm, (b) 1250-mm, (c) 1000-mm, (d) 850-mm and (e) 630-mm diameter ingot

2) Defects size ranges of 10~40 μm and greater than 40 μm were analyzed, the results suggesting that defects of sizes greater than 40 μm account for the largest proportion among the counted two kinds of defects.
3) The distribution of defects that greater than 40 μm along the radial direction was detected, its area fraction increases as its distance from the side, that is to say micro-defects greater than 40 μm distributed the most in the center zone of ingots. The larger the ingot diameter, the more obvious the tendency was.

Acknowledgement

The authors gratefully acknowledge the financial supports from NNSFC (Grant No. U1637601), CALT (Grant No. 20171038-056), Nonferrous Metal Oriented Advanced Structural Materials and Manufacturing Cooperative Innovation Center of Central South University and Guangxi Liuzhou Yinhai Aluminum Co., Ltd. Support and valuable discussion with Mr. Guangze Jia was greatly appreciated.

REFERENCES

[1] P.E. Krajewski, J.E. Allison, J.W. Jones, The influence of matrix microstructure and particle reinforcement on the creep behavior of 2219 aluminum [J]. Metallurgical Transactions A **24** (12), 2731-2741 (1993).

[2] G.M. Vyletel, J.E. Allison, D.C.V. Aken, The effect of matrix microstructure on cyclic response and fatigue behavior of particle- reinforced 2219 aluminum: Part I. room temperature behavior [J]. Metallurgical & Materials Transactions A **26** (12), 3143-3154 (1995).

[3] H. Wang, Y. Yi, S. Huang, Investigation of quench sensitivity of high strength 2219 aluminum alloy by TTP and TTT diagrams [J]. Journal of Alloys & Compounds **690**, 446-452 (2017).

[4] R. Francis, Quality control and improvement of the aluminum alloy castings for the next generation of engine block cast components [J]. **75** (3), 194-225 (2005).

[5] S. Kumai, J. Hu, M. Ishikura, Y. Higo, S. Nunomura, Effects of solidification structure on tensile properties in SiC particulate-reinforced cast aluminum alloy composites [J]. Journal of Japan Institute of Light Metals **44** (4), 222-228 (1994).

[6] C. Gras, M. Meredith, J.D. Hunt, Microdefects formation during the twin-roll casting of Al-Mg-Mn aluminium alloys [J]. Journal of Materials Processing Technology **167** (1), 62-72 (2005).

[7] V.I. Betekhtin, A.G. Kadomtsev, P. Král, J. Dvořák, M. Svoboda, I. Saxl, V. Sklenička, Significance of Microdefects Induced by ECAP in Aluminium, Al-0.2%Sc Alloy and Copper [J]. Materials Science Forum **567-568**, 93-96 (2007).

[8] A.H. Patel, Mathematical modeling of microshrinkage formation during solidification of A356 alloy castings [J]. Dissertations & Theses – Gradworks **8** (1), 21-27 (2013).

[9] L. Liu, A.M. Samuel, F.H. Samuel, H.W. Doty, S. Valtierra, Influence of oxides on porosity formation in Sr-treated Al-Si casting alloys [J]. Journal of Materials Science **38** (6), 1255-1267 (2003).

[10] S. Narisawa, H. Yoshino, Y. Hirakawa, K. Noda, Porosity-Controlled Ethylcellulose Film Coating. I. Formation of Porous Ethylcellulose Film in the Casting Process and Factors Affecting Film-Density [J]. Chemical & Pharmaceutical Bulletin **41** (2), 329-334 (2008).

[11] P. Robichaud, C. Dupuis, A. Mathis, P. Côté, B. Maltais, In-Line Salt-ACD™: A Chlorine-Free Technology for Metal Treatment[J]. Tms Light Metals **49**(6), 737-742 (2011).

[12] X. Liu, Y. Li, X. Chen, Bubble size control during the gas injection foaming process in aluminum alloy melt [J]. Journal of Materials Research **30** (7), 1002-1010 (2015).

[13] A.G. Szekely, The removal of solid particles from molten aluminum in the spinning nozzle inert flotation process [J]. Metallurgical Transactions B **7** (2), 259-270 (1976).

[14] H. Jung, E.S. Savage, Deep-Bed Filtration [J]. Journal **66** (2), 73-78 (1974).

[15] D.P. Lapham, C. Schwandt, M.P. Hills, R.V. Kumar, D.J. Fray, The detection of hydrogen in molten aluminium [J]. Ionics **8** (5-6), 391-401 (2002).

[16] M. LI G.R.I. L. Liquid Metal Cleaniness Analyzer (LiMCA) in Molten Aluminum [J]. Transactions of the Iron and Steel Institute of Japan (2), 101-110 (2001).

[17] C. Stanică, P. Moldovan, Aluminum melt cleanliness performance evaluation using PoDFA (porous disk filtration apparatus) technology [J]. Upb Scientific Bulletin **71** (4), 107-114 (2009).

[18] X. Cao, Mechanisms of pressure filtration of liquid aluminum alloys [J]. Metallurgical & Materials Transactions B **37** (6), 1075-1083 (2006).

[19] W. Harara, Digital radiography of aluminum castings by fluoroscopy [J]. Russian Journal of Nondestructive Testing **48** (6), 384-390 (2012).

[20] O. Lashkari, L. Yao, S. Cockcroft, D. Maijer, X-Ray Microtomographic Characterization of Porosity in Aluminum Alloy A356 [J]. Metallurgical & Materials Transactions A **40** (4), 991-999 (2009).

[21] J. Mathew, A. Mandal, J. Warnett, M.A. Williams, M. Chakraborty, P. Srirangam, X-ray tomography studies on porosity and particle size distribution in cast in-situ Al-Cu-TiB 2 semi-solid forged composites [J]. Materials Characterization **118**, 57-64 (2016).

[22] S.W. Hudson, D. Apelian, Inclusion Detection in Molten Aluminum: Current Art and New Avenues for In Situ Analysis [J]. International Journal of Metalcasting **10** (3), 289-305 (2016).

[23] T.L. Mansfield, Ultrasonic Technology for Measuring Molten Aluminum Quality [J]. JOM **34** (9), 54-57 (1982).

[24] R.G. Maev, J.H. Sokolowski, H.T. Lee, E.Y. Maeva, A.A. Denissov, Bulk and subsurface structure analysis of the 319 aluminum casting using acoustic microscopy methods [J]. Materials Characterization **46** (4), 263-269 (2001).

[25] A.S. Kim, K.D. Stolzenbach, Aggregate formation and collision efficiency in differential settling [J]. J Colloid Interface Sci **271** (1), 110-119 (2004).

[26] A. Mitrasinovic, F.C.R. Hernández, M. Djurdjevic, J.H. Sokolowski, On-line prediction of the melt hydrogen and casting porosity level in 319 aluminum alloy using thermal analysis [J]. Materials Science & Engineering A **428** (1-2), 41-46 (2006).

[27] M. Xiong, A.V. Kuznetsov, Comparison between Lever and Scheil Rules for Modeling of Microporosity Formation during Solidification [J]. Flow Turbulence & Combustion **67** (4), 305-323 (2001).

[28] T. Magnusson, L. Arnberg, Density and solidification shrinkage of hypoeutectic aluminum-silicon alloys [J]. Metallurgical & Materials Transactions A **32** (10), 2605-2613 (2001).